CFD Simulations of Vehicle Self-Soiling

Martin Ševčík[1], Rene Devaradja[1], Martin Novák[1], Jacques Papper[1] and Martin Černý[2]

[1]Icon Technology & Process Consulting Ltd.
[2]ŠKODA AUTO a. s.

m.sevcik@iconcfd.com
r.devaradja@iconcfd.com
m.novak@iconcfd.com
j.papper@iconcfd.com
Martin.Cerny2@skoda-auto.cz

Abstract: Self-soiling occurs when dirt and water from the road are lifted by the wheels and deposited onto the vehicle body. This phenomenon affects visibility, sensor functionality, and driving safety. Addressing contamination issues late in the development cycle can result in increased costs and project delays. Computational fluid dynamics (CFD) provides a cost-effective alternative, enabling early identification of contamination patterns through virtual prototyping.

This study investigates vehicle contamination using CFD simulations performed with iconCFD. The external airflow was coupled with a discrete particle phase, where water droplets were modelled as Lagrangian particles, and a film model was applied to track droplet deposition on the vehicle surface.

The CFD results were validated against experimental data from the FKFS climatic wind tunnel by analysing the effects of wheel size, rim design, and mudguards on surface contamination. Different methods for simulating rotating wheels were compared to assess their influence on accuracy. The reliability of airflow predictions was confirmed by comparing CFD-derived pressures with experimental data from sensors positioned at hundreds of locations on the vehicle. Contamination predictions were evaluated by comparing simulated soiling patterns with image data from wet-condition experiments. The findings demonstrate the effectiveness of CFD in predicting vehicle contamination, supporting improved sensor performance and overall cleanliness.

1. Introduction

1.1 Background and Motivation

Vehicle soiling is a critical factor in aerodynamic development, impacting driver visibility, passenger comfort, and, most importantly, safety. Reliable sensor performance and unobstructed sightlines are essential for modern vehicles, particularly those equipped with advanced driver-assistance systems (ADAS). Experimental testing, whether in wind tunnels or on-road, requires a full prototype and specialized facilities, making it costly and often infeasible early in the design cycle. In contrast, virtual simulation methods enable rapid evaluation of design changes from the outset, although they must be validated against experimental data to ensure accuracy.

1.2 Exterior Water Management and Vehicle Soiling Sources

The study of exterior water management (EWM) encompasses multiphase flow involving the carrier airflow, spray particles, surface flows, and their interactions [1]. Vehicle soiling arises from several sources, as illustrated in Figure 1. Wind-driven rain produces relatively large droplets that impact the windshield, side windows, A-pillars, and mirrors. Additional contamination comes from other road users, where smaller droplets are lifted from the road surface by surrounding vehicles and deposit on similar areas as rain. Self-soiling occurs when the vehicle's own wheels generate liquid mist and debris, primarily affecting the wheelhouses, the full side panels, and the rear sections of the vehicle. These sources create characteristic soiling patterns due to differences in droplet size, deposition zones, and fluid dynamics, which must be understood to develop accurate predictive models and effective EWM strategies.

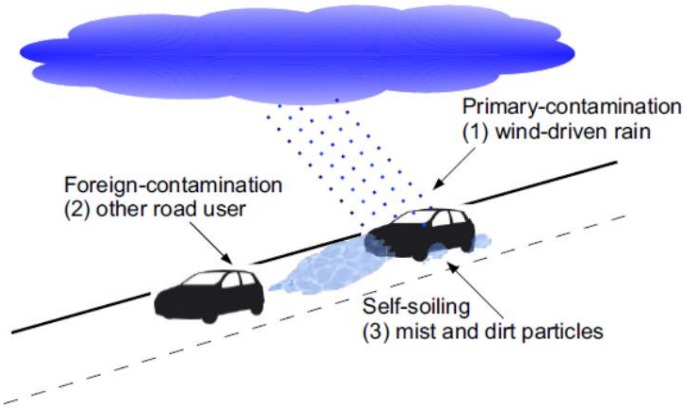

Figure 1 Vehicle soiling sources [1]

1.3 Previous Work and Validation Methods

Research to date has largely focused on external soiling, particularly rain. Novak et al. (2019 [2]) developed a validated Lagrangian–Eulerian methodology, tracking droplets in a Lagrangian frame while resolving airflow in an Eulerian frame.

Upon impact, droplets form a wall film modelled using Bai and Gosman's Continuous Phase Film Model (CPFM) [3], which assumes a quadratic velocity profile in the wall-normal direction, enabling efficient simulation with minimal computational cost.

The model accounts for hydrostatic and capillary pressures, shear stresses from air and wall interactions, gravitational forces, droplet momentum, and partial wetting through a dynamic contact angle with hysteresis and precursor film thickness. Realistic windscreen wiper motion is simulated using an Immersed Boundary Method (IBM), providing accurate wiper-induced water transport with minimal computational overhead as demonstrated in [2].

Coupling between the droplet and airflow phases is handled in two ways. One-way coupling neglects droplet feedback on the airflow, allowing to keep the carrier flow field frozen and computing only droplet and film motion, which is efficient for air-driven film flows such as along A-pillars and side windows. Two-way coupling accounts for droplet feedback on the airflow, providing higher accuracy in areas of high mist density at increased computational cost; this approach is used for predicting mirror contamination and self-soiling.

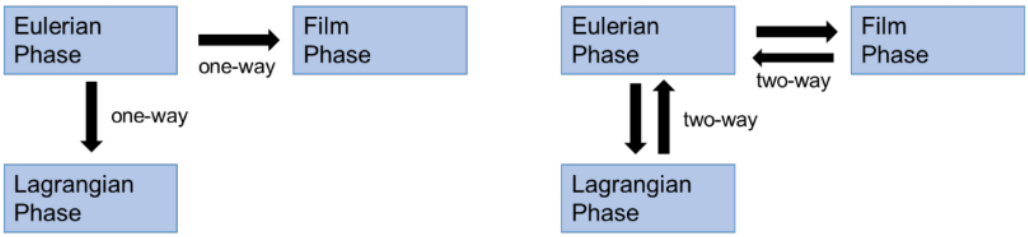

Figure 2 Coupling options between air, particles and film

Self-soiling mechanisms were investigated experimentally by Strohbücker et al. (2019 [4]) using rotating kart tires. Their results shown that tires act as rotary atomizers: water lifted from the road forms ligaments via Rayleigh–Taylor instabilities, which break into droplets through Rayleigh–Plateau mechanisms. The resulting droplet distribution peaks around 0.2 mm, with higher tire speeds increasing the number of smaller droplets while maintaining the most common diameter. Distinct spray zones were observed, as depicted in Figure 3, with the splash/spray region behind the contact patch carrying most of the water mass and larger droplets.

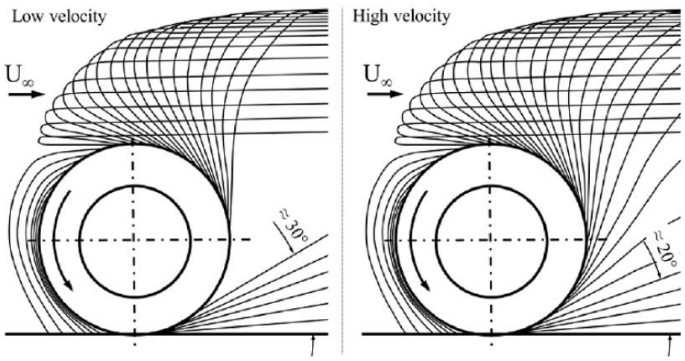

Figure 3 Schematic of droplet field for a free rolling grooved tire at low and high velocities [4]

Tread design significantly affects droplet formation: grooved tires maintain ligament formation at high speeds, whereas slick tires lose water earlier, reducing droplet mass in the second half

of rotation. These experimental findings provide a robust dataset for validating self-soiling simulations and suggest that mechanisms observed in kart tires can be applied to full-scale vehicles under typical operating conditions.

2. Experimental Setup

The FKFS thermal wind tunnel in Stuttgart, represented in Figure 4, was used for experimental validation. This Göttingen-type tunnel features a 2-axis dynamometer test bench but lacks a central belt under the car. The test section dimensions are 15.8 m × 6.8 m × 5.5 m. A water film is applied to rollers beneath the wheels via an irrigation system. The rotating wheels lift the water, generating a droplet field. A UV-tracer fluid is added to the water to visualize its motion on the vehicle surfaces. During testing, tunnel lights are switched off and UV lights illuminate the areas of interest. UV cameras capture the water flow across the vehicle surfaces. Between tests, the vehicle is cleaned with a water jet and dried with compressed air. Nevertheless, fully draining the wind tunnel test section between tests is practically infeasible. This introduces additional, and somewhat arbitrary, sources of water specific to the wind tunnel design, which should be considered when analysing the simulation results.

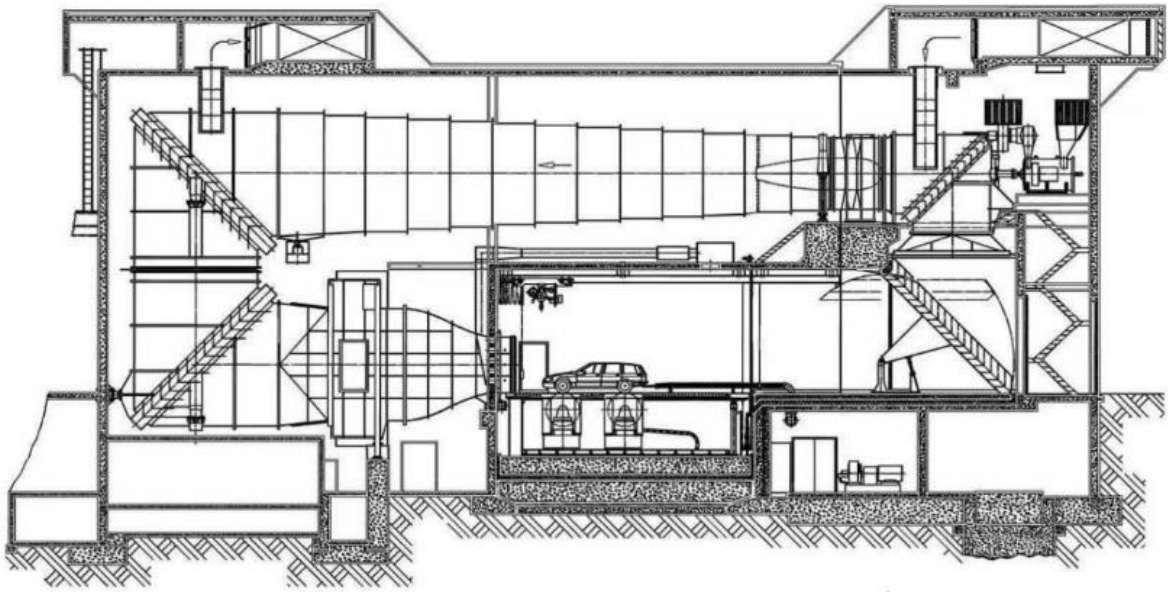

Figure 4 FKFS thermal wind tunnel diagram [5]

Accurate prediction and validation of the flow field are critical for reliable soiling simulations. Therefore, the experiment was divided into two parts: validation of external aerodynamics and validation of soiling. For aerodynamic validation, pressure strips were employed. These MEMS-based digital sensors [6], shown in Figure 5, measure absolute pressure at 100 Hz sampling frequency. The data averaged over the last 15s were used for validation. Their non-intrusive installation eliminates the need for drilling into the vehicle body. Each strip is 255.6 mm long and contains 24 pressure sensors. Ten strips were mounted on the vehicle, with two additional reference strips positioned inside the tunnel test section behind the nozzle.

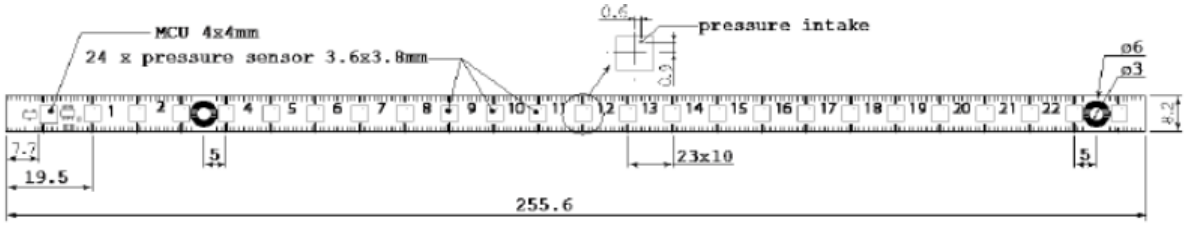

Figure 5 Pressure strip schematics and dimensions [6]

A production Skoda Kodiaq SUV was selected for testing. Since the focus was on self-soiling, different wheel and tire combinations were evaluated. As shown in Figure 6, two wheel sizes R17 (1) and R19 (2) were used and two other wheel variants of R19 were also tested by adding rim covers (3) and optional mud flaps (4). Four airspeeds values 70, 90, 110, and 130 km/h were measured for each configuration.

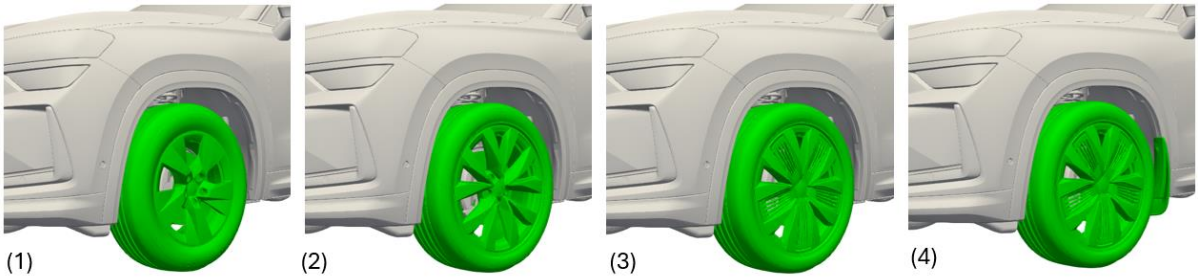

Figure 6 Tested wheel variants

Preliminary CFD simulations, previously validated for A-pillar overflow, were performed to determine optimal pressure strip locations. The first strip (P1) was positioned on the registration plate to capture stagnation pressure and calculate the pressure coefficient. The second strip (P2) was mounted on the leading edge of the roof, just behind the windscreen edge. The remaining strips were distributed across four areas: behind the front left wheel (P3, P4, side panel), underbody left floor covers (P5, P6), inside the front left wheel arch (P7, P8), and around the rear wheel (P9, P10). All these strip positions are shown in Figure 7.

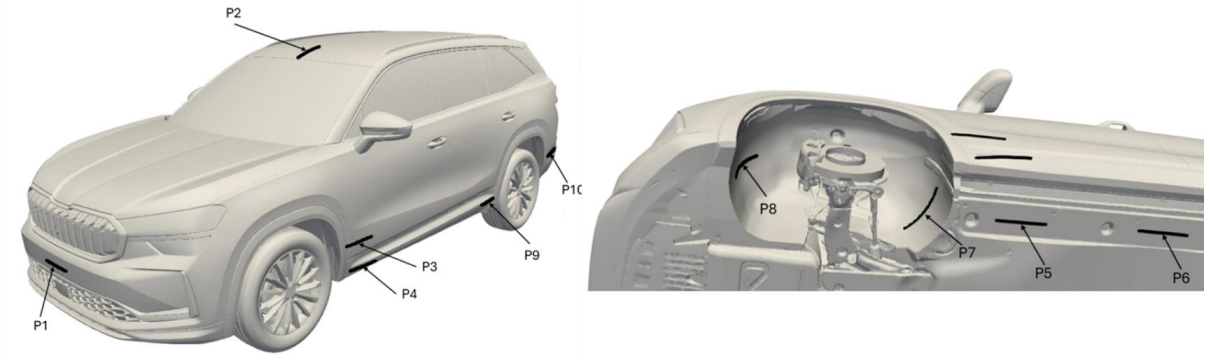

Figure 7 Pressure strip locations on the vehicle

Soiling measurements focused on two main areas: the side doors and rear part of the vehicle. Each area required a dedicated injector configuration and camera placement and was tested separately. Measurement variants differed in wind speed, water mass flow, wheel configuration, and the presence or absence of mudguards. A detailed test matrix is provided in Table 1.

Type	Speed [km/h]	Water amount [l/h]	R17 Mudguards		R19 Mudguards		R19 + inserts Mudguards	
			Yes	No	Yes	No	Yes	No
Side	70	140 (F), 200 (R)					x	x
		200 (F), 250 (R)						
	90	140 (F), 200 (R)	x		x		x	x
		200 (F), 250 (R)					x	x
	110	140 (F), 200 (R)	x		x		x	x
		200 (F), 250 (R)					x	x
	130	140 (F), 200 (R)					x	x
Rear	90	600 (R)	x		x		x	x
		400 (R)						x
	110	600 (R)	x		x		x	x
		400 (R)						x

Table 1 Testing configurations for side and rear soiling analysis

3. CFD Methodology and Setup

The virtual wind tunnel was simulated using the finite volume CFD software iconCFD v4.2.12. The computational domain is a rectangular box with a velocity inlet and pressure outlet, including rolling pads under the wheels to model ground interaction via tangential velocity boundary conditions. The central belt was omitted, matching the FKFS climatic wind tunnel setup. The remaining floor surfaces were modelled as no-slip walls.

The computational mesh is unstructured and hexa-dominant, with 4 prism layers on the vehicle surfaces and 7 prism layers on the wheels. Unsteady simulations are required to capture the external aerodynamics accurately ([2], [7], [8]). The workflow was initialised with a steady-state RANS initialization, followed by a transient DDES simulation using incompressible, pressure-based segregated solvers. The transient phase lasted 1.4 s, with the first 0.4 s used to transition from the RANS solution to a fully transient state, and the remaining 1 s used for averaging the results. Both stages employed the Spalart – Allmaras turbulence model [9].

Previous methodologies focused on the A-pillar and rear-view mirror regions, enabling significant simplifications—such as excluding wheel rotation, engine bay flow, and heat exchanger modeling and underbody flow resolving with reduced detail. These simplifications substantially reduced computational cost without compromising the fidelity of the targeted flow features. For the current self-soiling study, all these features were incorporated: the engine bay was open, heat exchangers were represented as porous media, and airflow through the engine compartment and underbody was fully resolved. Wheel rotation was modelled using two approaches: a Moving Reference Frame (MRF) and physical mesh rotation with an Arbitrary Mesh Interface (AMI). The latter is theoretically more accurate but computationally more expensive. Finally, the tires were deformed to reproduce their realistic shape, as shown in Figure 8. To ensure an accurate representation, the car in the CFD model was positioned according to ride height data obtained from wheel arch apex measurements in the wind tunnel.

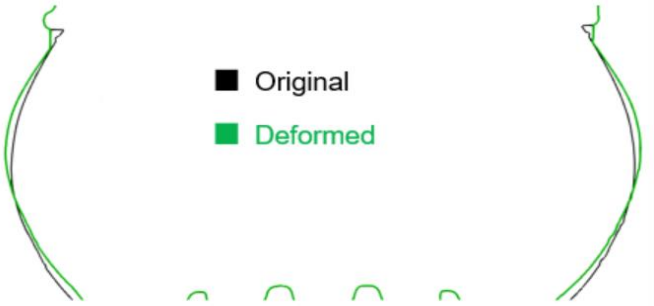

Figure 8 Tire deformation on 17″ wheels

The soiling process was modelled using an unsteady multiphase solver with two-way coupling between the Eulerian and Lagrangian phases. Surface wetting was captured using a continuous-phase film model [2], [11]. The wall interaction model assumed that particles adhered upon contact with the surface, and breakup caused by airflow shear forces was modelled using the Reitz–Diwakar approach [10]. The particle equation of motion accounted for gravity, aerodynamic drag, and pressure gradient forces, and detachment from the surface film was represented through mechanisms such as wave stripping, edge shedding, curvature separation, and gravity-induced separation [12]. Together, these processes reproduced realistic droplet behaviour. Water particles were injected from the start of the unsteady simulation via conical injectors placed behind the tire contact patch and on the tire surface itself [4], with particle diameters set to 0.2 mm. Each soiling measurement in the wind tunnel lasted 3 minutes, whereas the CFD simulations were limited to 20 s transient DDES runs initialized with steady-state RANS. To compensate for the shorter simulation duration, the water mass flow rate was proportionally increased, although this adjustment can influence the soiling distribution, as wetted surfaces may absorb more of the dispersed water. It can also be noted that, in the wind tunnel, redeposition from the vehicle, the tunnel floor, or the rolling pads represents a possible additional source of contamination.

4. Validation

4.1 External aerodynamics

Two locations were selected to verify pressure levels in the domain: the registration plate (P1), corresponding to a stagnation point with a pressure coefficient around 1, and the leading edge of the roof (P2), where no separation is expected and the pressure gradient is relatively mild. Experimental and CFD results agreed very well at both locations across all wheel variants. An example for the 17″ wheels at 70 km/h is shown in Figure 9.

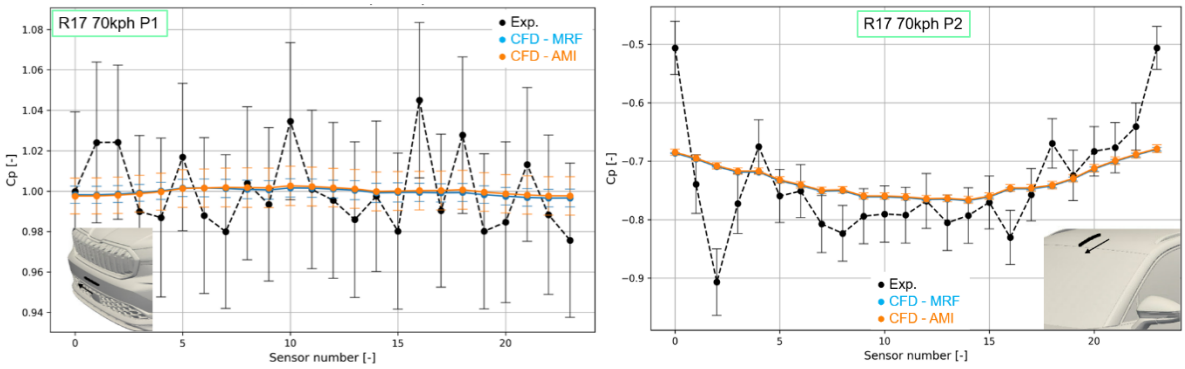

Figure 9 Pressure coefficient prediction for R17 - 70kph - P1 and P2

The main area of interest is the side of the vehicle between wheel arches, where airflow is strongly influenced by wheel rotation. Both the MRF and AMI approaches produced very similar pressure distributions. Agreement with experimental data is excellent in observed locations, as shown in Figure *10*, indicating that the CFD methodology enables accurate airflow prediction, providing a reliable basis for self-soiling analysis.

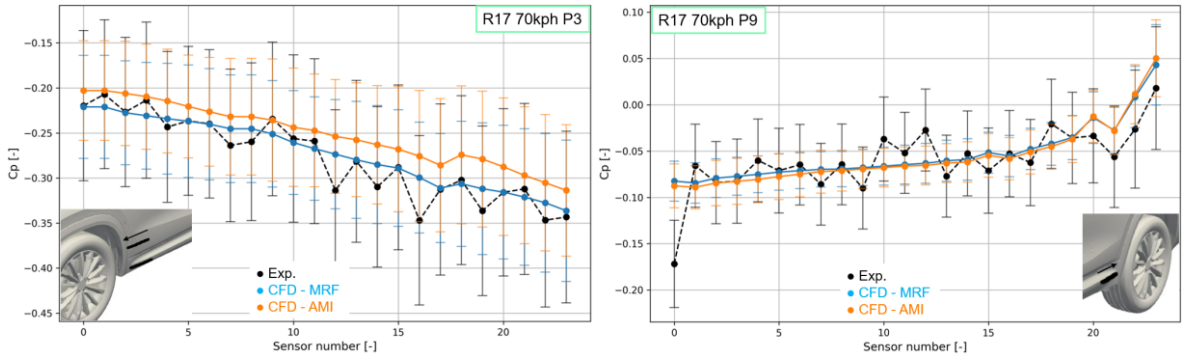

Figure 10 Pressure coefficient prediction for R17 – 70 kph – P3 and P9

In contrast, discrepancies were observed inside the wheel arch and on the floor cover near the wheel, as illustrated in Figure *11*. These differences are likely due to the tire wake from the contact patch not being accurately captured. While the trend matches the experiments, CFD consistently under predicts absolute values of static pressure. Correlation improves further along the floor cover (P6). Additional factors contributing to these discrepancies may include the simplified tire tread geometry, the absence of validated boundary layers on the tunnel floor, and the simplified representation of engine bay airflow.

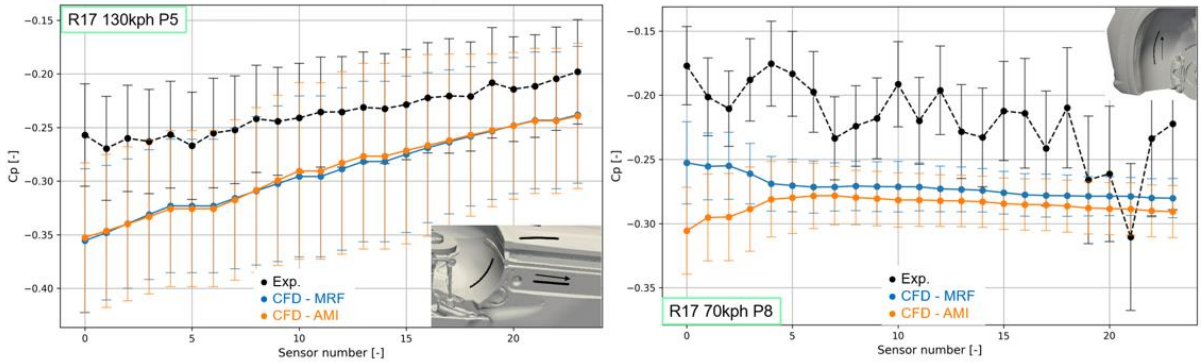

Figure 11 Pressure coefficient prediction for R17 – 130 kph – P5

4.2 Soiling validation

The experimental data from Figure *12* and Figure *13* confirm the findings of Strohbücker et al. (2019, [4]): at higher speeds, the spray angle decreases, leading to reduced surface contamination. To reproduce the same trend in CFD, the injector cone angle was manually adjusted—set to 30° for 70 and 90 kph, and to 20° for 110 and 130 kph. Although this manual adjustment is not ideal for a general self-soiling methodology, it was used as an attempt to replicate the experimental results in CFD and to demonstrate that the injector cone angle has a dominant effect on surface contamination. However, differences in contamination intensity can be observed at all speeds. The experiments also show a larger contaminated area at lower speeds (70 and 90 kph), whereas this effect was not captured in the CFD simulations. This indicates that further adjustments to the cone injector are potentially required. It also highlights

the need for an enhanced water injection method allowing for non-uniform injection distribution from the wheel surface that accounts for the physical phenomena described in [4].

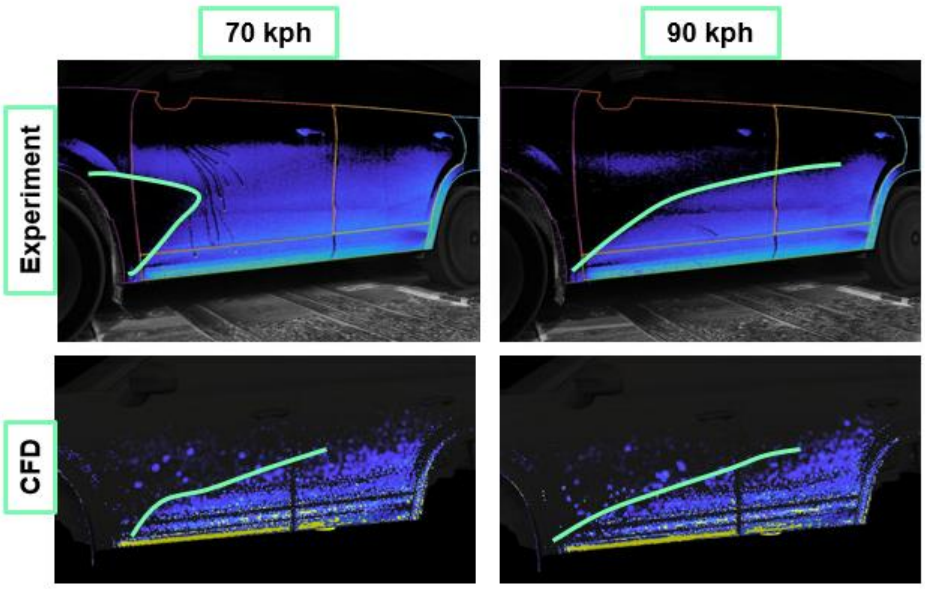

Figure 12 Configuration R19 with covers and mudguards – 70 and 90 kph

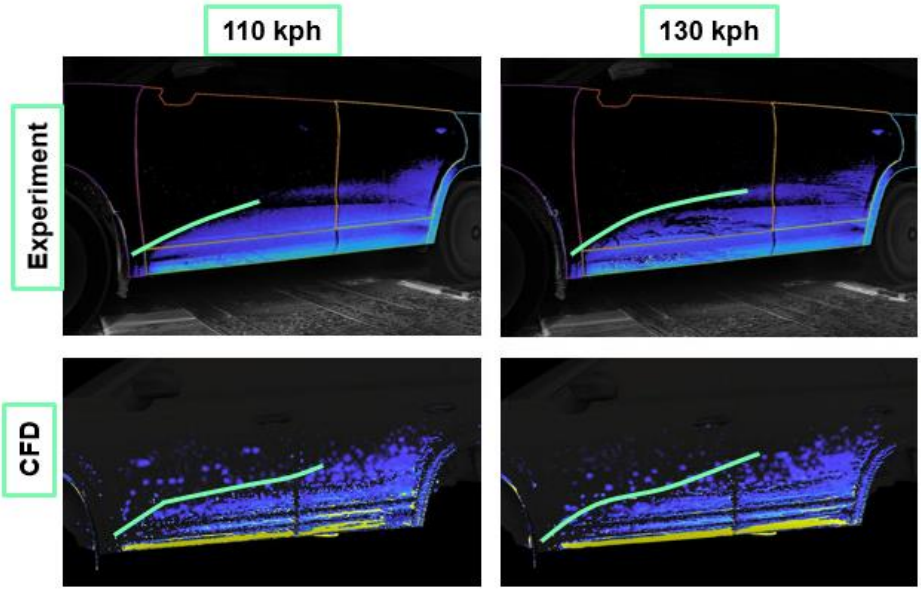

Figure 13 Configuration R19 with covers and mudguards – 110 and 130 kph

The influence of mudguards is also noticeable in Figure *14*. The addition of mudguards reduces the overall contaminated area, while increased contamination intensity can be observed at the edge of the door sill. CFD reproduces this trend moderately, but differences in contamination intensity can still be observed. Additionally, the separation line between the wetted and dry zones without mudguards is slightly lower than in the experiment.

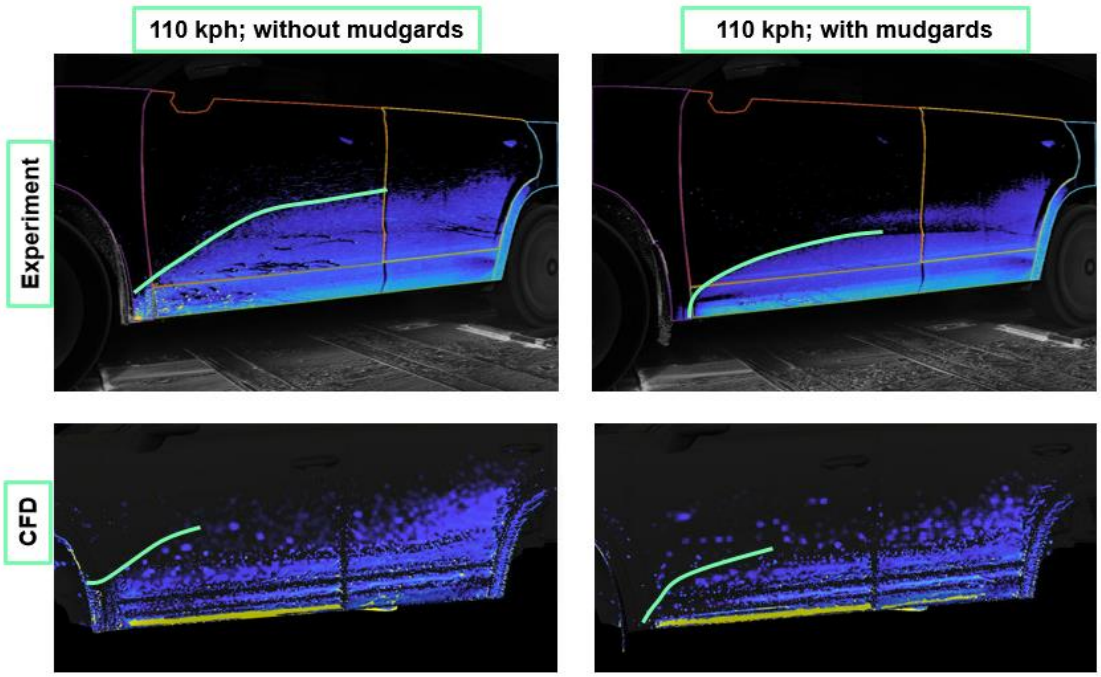

Figure 14 Configuration R19 with covers – mudguards effects

The influence of different wheel designs is also significant, as shown in Figure *15*. The highest level of contamination occurs with the 17" wheels. Adding covers to the 19" wheels alters the shape of the spray-free triangle, but has little effect on the overall contaminated area. Contamination at the edge of the door sill increases with the cover installed. CFD reproduces the change in the shape of the spray-free triangle moderately well, but the overall contamination levels differ from the experiment, being lowest for the 17" wheels. This likely points to the need of the aforementioned advanced wheel surface injector inclusion. It shall be noted that CFD predicts well the dry spots occurring in the bottom half of the front door with 17" wheels

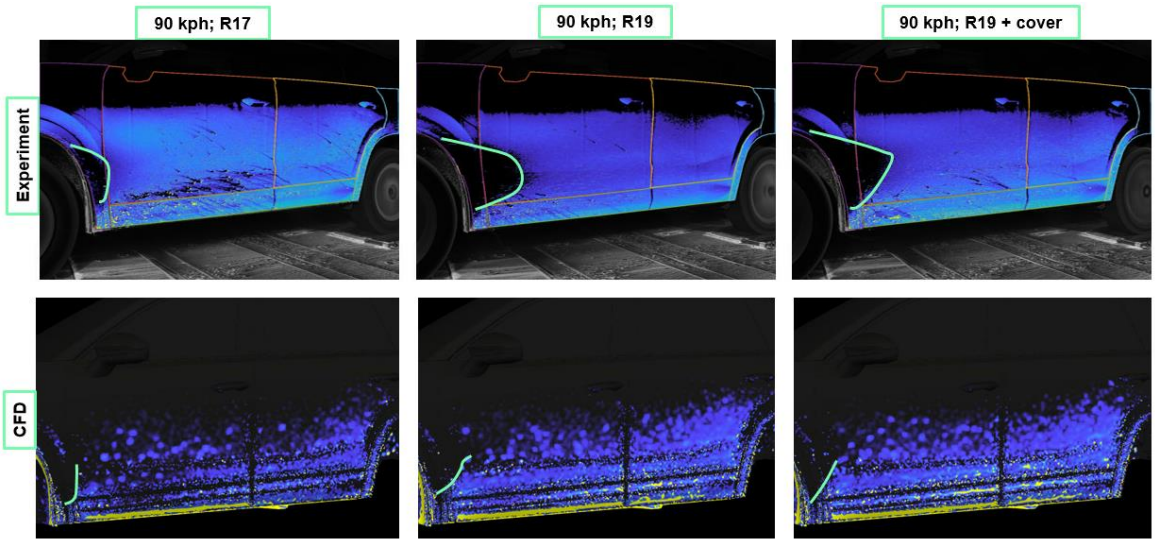

Figure 15 Surface contamination for different wheel designs

Experimentally, the central portion of the rear soiling pattern remained consistent across all tested variants. Among the configurations, the R17 wheels generated the largest contamination-free zones near the rear edges, while the introduction of R19 wheel covers and the addition of mudguards had minimal impact on the soiling patterns at the rear. CFD captures some general trends, predicting similar contamination patterns for the other R19 configurations. However, it

fails to reproduce key features observed in the experiments, such as the differences at the rear bottom-side edges, and exhibits noticeable asymmetry for the R17 configuration that is not present in the measurements. The absence of data in this region does not allow us to determine whether these discrepancies arise from an inaccurate airflow simulation or from limitations in the soiling model itself, highlighting the need for further investigation.

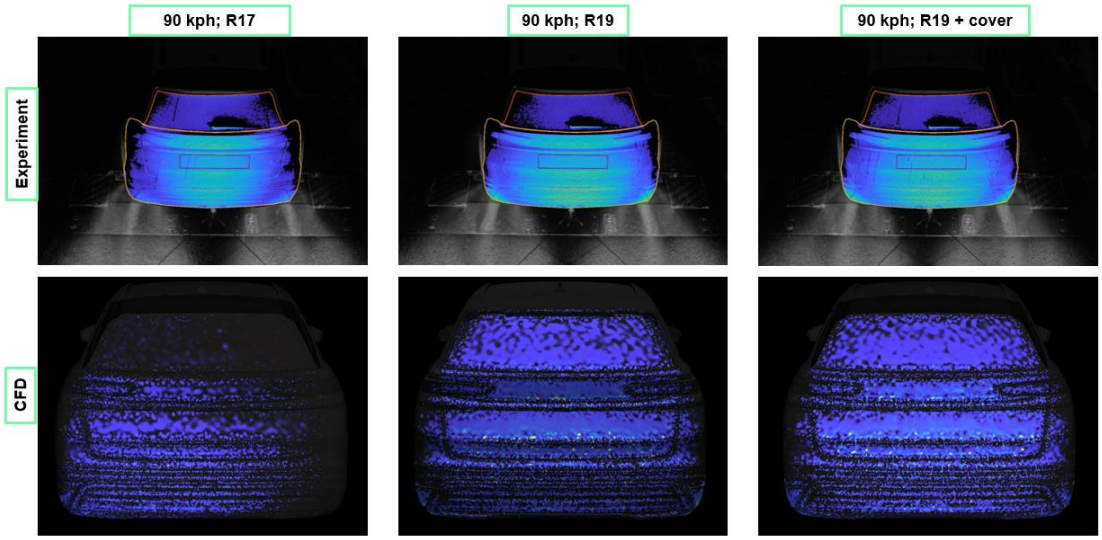

Figure 16 Rear contamination for different wheel designs

5 Summary

The goal of this study was to develop a reliable and experimentally validated simulation methodology for vehicle self-soiling, where water lifted by the wheels contaminates the vehicle body. Simulations were performed using transient Delayed Detached Eddy Simulation (DDES) solver with the Spalart–Allmaras turbulence model, modelling wheel rotation via both Moving Reference Frame and Arbitrary Mesh Interface techniques. Soiling was simulated using a two-way coupled Lagrangian-Eulerian framework, with droplet emission from both conical injectors and tyre surface. Surface film dynamics were captured via the Continuous Phase Film Model.

CFD predictions of external airflow matched experimental data well in most regions, particularly on the side panels and roof. Both MRF and AMI produced comparable results, with MRF chosen for soiling simulations due to lower computational cost. Some discrepancies were noted in the wheel arch and underbody areas, which are less critical for side and rear soiling.

Overall, CFD captured the qualitative trends observed experimentally, including reduced contamination behind the wheels at higher speeds and the effect of mudguards in limiting contaminated areas. Adjusting the injector cone angle successfully replicated the change in spray angle and contamination patterns at different speeds, though discrepancies in contamination intensity remain to be addressed. Accurate modelling of water expelled from the tire, dependent on tread and injection parameters, is still needed.

Wheel design effects were partially reflected in CFD, with some differences between R17 and R19 wheels captured, but the effect of adding R19 wheel covers was not sufficiently

reproduced. Quantitative contamination levels also differed, with CFD underestimating contamination for 17" wheels compared to experiments. These findings highlight the importance of refining injector settings and incorporating a more detailed tire surface representation with keeping in mind much shorter simulations than experiment to improve CFD accuracy in predicting vehicle self-soiling.

6 Acknowledgements

The authors gratefully acknowledge ŠKODA AUTO for granting permission to publish this work and for their excellent collaboration throughout the study.

References

[1] T. Hagemeier, Experimental and numerical investigation of vehicle soiling processes, 2012

[2] M. Novak, R. Devaradja, J. Papper, M. Cerny, Efficient CFD methods for assessment of water management, 2019

[3] C. Bai, A. D. Gosman, Mathematical Modelling of Wall Films Formed by Impinging Sprays. SAE Transactions, 105, 782–796. http://www.jstor.org/stable/44736317, 1996

[4] V. Strohbücker, R. Niesner, D. Schramm, T. Kuthada et al., Experimental Investigation of the Droplet Field of a Rotating Vehicle Tyre, SAE Technical Paper 2019-01-5068, 2019, doi:10.4271/2019-01-5068.

[5] N. Kruse and K.-H. Chen, Exterior Water Management Using a Custom Euler-Lagrange Simulation Approach, in SAE World Congress & Exhibition, 2007

[6] F. Wittmeier, T. Kuthada, J. Filipsky and J. Cizek, New MEMS Pressure Sensors for Transient Aerodynamic Measurements, ATZ worldwide, vol. 120, pp. 38-41, 4 2018.

[7] T. Han, S. Kaushik, K. Karbon, B. Leroy, K. Mooney, S. Petropoulou and J. Papper, Ad-joint-Driven Aerodynamic Shape Optimization Based on a Combination of Steady State and Transient Flow Solutions, 2016.

[8] R. Lietz, L. Larson, P. Bachant, J. Goldstein, R. Silveira, M. Shademan, P. Ireland and K. Mooney, An Extensive Validation of an Open Source Based Solution for Automobile External Aerodynamics, in WCX™ 17: SAE World Congress Experience, 2017.

[9] P.R. Spalart and S.R. Allmaras. A One-Equation Turbulence Model for Aerodynamic Flows. Recherche Aerospatiale, 1:5–21, 1994

[10] R.D. Reitz, R. Diwakar, Effect of Drop Breakup on Fuel Sprays, SAE Paper 860469, 1987.

[11] P.T. Brun, A. Damiano, P. Rieu, G. Balestra, F. Gallaire, Rayleigh-Taylor instability under an inclined plane.Physics of Fluids (1994-present), 27(8), 084107.

[12] K. Meredith, J. Vries and Y. Xin, A numerical model for partially-wetted flow of thin liquid films, 2011.